

THE RADIO ACTIVITY-ROTATION RELATION OF ULTRACOOLED DWARFS

M. MCLEAN¹, E. BERGER¹, AND A. REINERS²

Draft version April 24, 2022

ABSTRACT

We present a new radio survey of about 100 late-M and L dwarfs undertaken with the Very Large Array (VLA). The sample was chosen to explore the role of rotation in the radio activity of ultracool dwarfs. As part of the survey we discovered radio emission from three new objects: 2MASS J0518113–310153 (M6.5), 2MASS J0952219–192431 (M7), and 2MASS J1314203+132001 (M7), and made an additional detection of LP 349-25 (M8). Combining the new sample with results from our previous studies and from the literature, we compile the largest sample to date of ultracool dwarfs with radio observations and measured rotation velocities (167 objects). In the spectral type range M0–M6 we find a radio activity-rotation relation, with saturation at $L_{\text{rad}}/L_{\text{bol}} \approx 10^{-7.5}$ above $v \sin i \approx 5 \text{ km s}^{-1}$, similar to the relation in H α and X-rays. However, at spectral types \gtrsim M7 the ratio of radio to bolometric luminosity increases significantly regardless of rotation velocity, and the scatter in radio luminosity increases. In particular, while the most rapid rotators ($v \sin i \gtrsim 20 \text{ km s}^{-1}$) exhibit “super-saturation” in X-rays and H α , this effect is not seen in the radio. We also find that ultracool dwarfs with $v \sin i \gtrsim 20 \text{ km s}^{-1}$ have a higher radio detection fraction by about a factor of 3 compared to objects with $v \sin i \lesssim 10 \text{ km s}^{-1}$. When measured in terms of the Rossby number (Ro), the radio activity-rotation relation follows a single trend and with no apparent saturation from G to L dwarfs and down to $Ro \sim 10^{-3}$; in X-rays and H α there is clear saturation at $Ro \lesssim 0.1$, with super-saturation beyond M7. A similar trend is observed for the radio surface flux (L_{rad}/R_*^2) as a function of Ro . The continued role of rotation in the overall level of radio activity and in the fraction of active sources, and the single trend of $L_{\text{rad}}/L_{\text{bol}}$ and L_{rad}/R_*^2 as a function of Ro from G to L dwarfs indicates that rotation effects are important in regulating the topology or strength of magnetic fields in at least some fully-convective dwarfs. The fact that not all rapid rotators are detected in the radio provides additional support to the idea of dual dynamo states proposed from spectropolarimetric observations.

Subject headings: radio continuum:stars — stars:activity — stars:low-mass, brown dwarfs — stars:magnetic fields

1. INTRODUCTION

Rotation plays a key role in the magnetic dynamos of cool stars. The $\alpha\Omega$ dynamo (Parker 1955) is the standard mechanism used to explain magnetic field generation in sun-like stars. The combination of winding of magnetic field lines due to differential rotation, and twisting by convective motions results in the generation of a magnetic field whose strength is highly dependent on stellar rotation. Indeed, this dynamo mechanism is supported by the observed correlation between rotation and magnetic activity (indicated by H α , Ca II H&K, X-rays, and radio), as well as between rotation and inferred magnetic field strengths (from Zeeman broadening) in F to early-M dwarfs (Noyes et al. 1984; Stewart et al. 1988; James et al. 2000; Delfosse et al. 1998; Pizzolato et al. 2003; Browning et al. 2010; Reiners et al. 2009; Morin et al. 2010). The critical parameter appears to be the Rossby number, $Ro = P/\tau_c$, where P is the rotation period and τ_c is the convective turnover timescale; magnetic activity increases with a decreasing Rossby number (e.g., Noyes et al. 1984). However, since the $\alpha\Omega$ dynamo operates at the transition layer between the radiative and convective zones in stars where differential rotation is maximized, a separate mechanism may be required to account for magnetic fields in fully-convective dwarfs (spectral types \gtrsim M3).

Observationally, H α and X-ray activity measurements

demonstrate that the correlation between rotation and activity continues beyond the expected transition to full convection (Delfosse et al. 1998; Mohanty & Basri 2003). However, since the activity in early- to mid-M dwarfs becomes saturated at a fairly low rotation rate, corresponding to $v \approx 5 \text{ km s}^{-1}$, few objects display the unsaturated correlation. An eventual breakdown in the saturated rotation-activity relation is observed in ultracool dwarfs (spectral type \gtrsim M7) in both X-rays and H α (e.g., Basri & Marcy 1995; Mohanty & Basri 2003; Berger et al. 2008), such that the activity levels decline precipitously in all objects, independent of rotation (e.g., Berger et al. 2010). A similar breakdown is seen in the correlation between rotation and magnetic flux Bf (Reiners & Basri 2010); here B is the magnetic field and f is the magnetic filling factor. Moreover, late-M dwarfs appear to exhibit distinct regimes of magnetic field topologies and strengths with no obvious correlation to the stellar rotation (Morin et al. 2010).

There are also hints of super-saturation among the most rapid rotators (with $v \gtrsim 20 \text{ km s}^{-1}$) where there appears to be a particularly strong suppression of H α (Reiners & Basri 2010) and X-ray (James et al. 2000; Berger et al. 2008) activity at spectral types beyond M7. It is unclear whether the super-saturation phenomenon is related to external effects such as centrifugal coronal stripping (Jardine & Unruh 1999; James et al. 2000; Berger et al. 2008), or to the actual generation of the magnetic field. Unfortunately, it is not possible to make direct magnetic flux measurements in rapidly rotating objects because Zeeman broadening is masked by rotational broadening (Morin et al. 2010; Reiners & Basri 2010).

¹ Harvard-Smithsonian Center for Astrophysics, 60 Garden Street, Cambridge, MA 02138

² Universität Göttingen, Institut für Astrophysik, Friedrich-Hund-Platz 1, 37077 Göttingen, Germany

Similarly, there is an inherent difficulty in using $H\alpha$ and X-ray emission to study field generation in ultracool dwarfs since the decrease in activity may be due to a decoupling between the increasingly neutral atmosphere and any existing magnetic fields (Mohanty et al. 2002), or to a change in the bulk coronal density (e.g., Berger et al. 2008). This is potentially manifested in the sharp breakdown of the tight radio/X-ray activity correlation (Guedel & Benz 1993; Benz & Guedel 1994) at spectral type M7 (Berger 2002, 2006; Berger et al. 2010). Thus, while X-ray and $H\alpha$ activity plummet in ultracool dwarfs, the ratio of radio to bolometric luminosity actually increases in the coolest objects, while the radio luminosity itself remains largely unchanged, at least to spectral type \sim L4 (Berger 2002, 2006; Berger et al. 2010). Thus, radio observations indicate that ultracool dwarfs are capable of generating stable large-scale kilo-Gauss magnetic fields. This result has been confirmed with Zeeman broadening observations of M dwarfs (Reiners & Basri 2010), as well as with magnetic topology studies using spectropolarimetry (Zeeman Doppler Imaging; Donati et al. 2006; Morin et al. 2010). However, radio activity remains a unique tool for studying the field topology and dissipation in rapid rotators.

Theoretical studies have led to several proposed models to explain the continued presence of magnetic fields in fully convective stars and brown dwarfs. Durney et al. (1993) proposed a turbulent dynamo that generates small-scale chaotic magnetic fields, with little dependence on rotation. However, this mechanism cannot produce sufficient large-scale magnetic fields to explain the observed Zeeman broadening, or the strong radio activity among ultracool dwarfs, particularly periodic radio emission that appears to require a substantial field with low multipole order (Berger et al. 2009; McLean et al. 2011). Chabrier & Küker (2006) explored the α^2 dynamo, which predicts large-scale primarily toroidal fields with a strong dependence on rotation, and saturation at high rotation rates where the α^2 mode becomes super-critical. This dynamo model has been proposed to dominate among all fast solid-body rotators, even the partially radiative early-M dwarfs. Dobler et al. (2006) conducted 3-dimensional hydrodynamic and magnetohydrodynamic (MHD) simulations of fully convective spheres, and found magnetic fields on all spatial scales, as well as differential rotation. They also found that the fields on the largest scales increase with rotation rate, reaching saturation only at fast rotation ($Ro \approx 0.01$), and exhibiting no sign of super-saturation. The MHD simulations of Browning (2008) also find that faster rotation produces higher magnetic energy densities, as well as magnetic fields on increasingly large-scales with a dipolar topology. However, their models do not include the fastest rotators.

In this paper, we study the relation between radio activity and rotation in M and L dwarfs as a way to explore and constrain the magnetic dynamo mechanism of ultracool dwarfs. A radio activity-rotation relation has been found in F–K stars (Stewart et al. 1988; Slee & Stewart 1989), as expected from the X-ray activity-rotation relation and the strong radio/X-ray correlation. Based on a small sample of ultracool dwarfs, Berger et al. (2008) found hints that a connection between radio activity and rotation may persist in late-M and L dwarfs, despite the breakdown in the $H\alpha$ and X-ray activity-rotation relations. Here we present a much larger sample of objects, taking advantage of new radio observations of 104 M and L dwarfs, as well as new rotation velocity measurements for previously-studied objects (Reiners & Basri 2008, 2010). We present the radio observations in §2, and new ultracool dwarf

detections in §3. In §4 we study the role of rotation in producing radio activity, and we discuss implications for dynamo models in §5. Our key finding is that the fastest rotators (highest $v\sin i$ and lowest Rossby number) have higher ratios of radio to bolometric luminosity, higher radio surface fluxes, and a higher radio detection fraction, suggesting that rotation continues to play a role in the magnetic dynamo mechanism of ultracool dwarfs.

2. OBSERVATIONS

We carried out a survey of 104 M and L dwarfs with the Very Large Array (VLA³). The properties of the sources are summarized in Table 1 and plotted in Figure 1. The targets are concentrated in the spectral type range M6–M9, where the X-ray/radio correlation and the X-ray/ $H\alpha$ activity-rotation relation break down. The sample includes sources with no previous radio observations, as well as several objects with previous detections or upper limits. The majority of the sample is located at $\lesssim 20$ pc. Taking into account objects with new velocity measurements that were observed in previous radio surveys, we have increased the number of objects with both radio and rotation measurements by about a factor of three compared to previous studies.

Each object was observed for 1 hr at 8.46 GHz using the standard continuum mode with 2×50 MHz contiguous bands. The flux density scale was determined using the extragalactic calibrators 3C 48 (J0137+331), 3C 138 (J0521+166), or 3C 286 (J1331+305), while the phase was monitored using calibrators located within 10° of the target sources. The data were reduced and analyzed using the Astronomical Image Processing System. The resulting flux density measurements are given in Table 1. Previous radio observations collection from the literature are presented in Table 2 (White et al. 1989; Krishnamurthi et al. 1999; Berger et al. 2001; Berger 2002; Burgasser & Putman 2005; Berger 2006; Phan-Bao et al. 2007; Berger et al. 2009).

3. NEW RADIO DETECTIONS

As part of this new survey we detect radio emission from four objects: 2MASS J0518113–310153 (M6.5), 2MASS J0952219–192431 (M7), 2MASS J1314203+1320011 (M7; McLean et al. 2011), and the previously-detected binary system LP 349-25 (M8; Phan-Bao et al. 2007). The measured flux densities are $181 \pm 27 \mu\text{Jy}$, $233 \pm 15 \mu\text{Jy}$, $1156 \pm 15 \mu\text{Jy}$, and $323 \pm 14 \mu\text{Jy}$, respectively. The fractional circular polarization for the four objects are $f_c \lesssim 45\%$ (2M0518–3101), $f_c \lesssim 30\%$ (2M0952–1924), $f_c = 18 \pm 2\%$ (2M1314+1320), and $f_c \lesssim 23\%$ (LP 349-25). These values are consistent with the level of circular polarization in the quiescent emission observed in other ultracool dwarfs (e.g., Berger 2002, 2006). The flux density measured for LP 349-25 is consistent with the value reported by Phan-Bao et al. (2007). No radio emission was detected from GJ 2005, BRI 0021-0214 or GJ 234A, despite previous radio detections (White et al. 1989; Berger 2002, 2006). Our upper limits for GJ 2005 and BRI 0021-0214 are only a factor of 1.7 and 1.4 below the previous detections, respectively. However, the upper limit on GJ 234A is almost 7 times below the detection from White et al. (1989), indicative of long-term variability.

We also carried out a 10 hr follow-up observation of 2M0952–1924 at 4.96 GHz and 8.46 GHz, but found no sig-

³ The VLA is operated by the National Radio Astronomy Observatory, a facility of the National Science Foundation operated under cooperative agreement by Associated Universities, Inc.

nificant detection, to a limit of $69 \mu\text{Jy}$, a factor of 2.4 below the original detection. This indicates that the initial detection was either a flare, or that the source experiences long-term variability. Since 2M 0952–1924 has a rotation velocity of $v\sin i \approx 6 \text{ km s}^{-1}$, its rotation period could be as long as 20 hr, indicating that the non-detection in 10 hr could also result from significant rotational modulation (Berger et al. 2005; Hallinan et al. 2006, 2007; Berger et al. 2009; McLean et al. 2011).

4. EXPLORING THE ROLE OF ROTATION

To explore the connection between rotation and radio activity we study the full sample of M and L dwarfs with radio observations and measured rotation velocities. In Figure 2 we plot the ratio of radio to bolometric luminosity as a function of spectral type for the full sample (Tables 1 and 2). We find an overall trend of increasing radio activity with later spectral type, at least to spectral type $\sim \text{L4}$, with a dearth of sources with $L_{\text{rad}}/L_{\text{bol}} \gtrsim 10^{-7}$ in spectral types earlier than M6 (see also Berger 2002, 2006). Moreover, essentially every detected object beyond a spectral type of M7 exhibits a value of $L_{\text{rad}}/L_{\text{bol}}$ that is larger than the saturated activity level in the M0–M6 dwarfs.

The distribution of rotation velocities as a function of spectral type is shown in Figure 3. There are no M0–M6 dwarfs with rotation velocities of $v\sin i \gtrsim 30 \text{ km s}^{-1}$, while among the ultracool dwarfs the sample is fairly uniformly distributed over the range of $\approx 5–60 \text{ km s}^{-1}$. Combining the rotation velocities with the radio luminosities (Figure 4), we find no clear correlation, although there is a tantalizing paucity of objects with $v\sin i \gtrsim 30 \text{ km s}^{-1}$ and radio luminosity of $\lesssim 10^{23} \text{ erg s}^{-1}$, which are present at $v\sin i \lesssim 30 \text{ km s}^{-1}$. The lack of an obvious change in radio luminosity from early-M dwarfs to ultracool dwarfs contrasts with the trends seen in $\text{H}\alpha$ and X-rays (Berger et al. 2010).

Since the X-ray and $\text{H}\alpha$ rotation trends are strongest when scaled relative to the bolometric luminosity, we plot $L_{\text{rad}}/L_{\text{bol}}$ as a function of rotation velocity in Figure 5. In the early- to mid-M dwarfs we find an apparent radio rotation-activity relation, with subsequent saturation at $v\sin i \gtrsim 5 \text{ km s}^{-1}$ and $L_{\text{rad}}/L_{\text{bol}} \approx 10^{-7.5}$. There are few detections below the saturation velocity, but the bulk of the upper limits for the slow rotators are well below the saturated emission level. This behavior is consistent with the rotation-activity relation observed in the X-rays, as expected from the radio/X-ray correlation in early-M dwarfs (Guedel & Benz 1993; Benz & Guedel 1994). It is also similar to the $\text{H}\alpha$ rotation-activity relation (Delfosse et al. 1998; Mohanty & Basri 2003). On the other hand, the detected late-M and L dwarfs exhibit a general increase in $L_{\text{rad}}/L_{\text{bol}}$ compared to M0–M6 (Figure 2). Therefore, the ultracool dwarfs no longer follow the saturation level observed in the early-M dwarfs, and instead reside at higher values of $L_{\text{rad}}/L_{\text{bol}} \sim 10^{-6.4}$. There is also an increase in the scatter of radio activity levels in ultracool dwarfs, similar to that seen in X-rays and $\text{H}\alpha$ (see Figure 6). The increased scatter is indicative of a breakdown in the correlation between the activity level and rotation velocity. On the other hand, at $v\sin i \gtrsim 20 \text{ km s}^{-1}$, where the X-ray and $\text{H}\alpha$ activity appear to exhibit super-saturation, there are indications of a trend towards higher radio activity levels (Figure 6). It is therefore clear that the radio activity and the $\text{H}\alpha$ /X-ray trends diverge in ultracool dwarfs, regardless of whether we normalize by the bolometric luminosity or not.

We further explore the role of rotation by investigating the

fraction of objects with radio detections as a function of rotation velocity. We divide the objects with spectral types M7–L4 into three $v\sin i$ bins, using two sets of binning, and retaining only significant non-detections, i.e., those with $L_{\text{rad}} \lesssim 2.5 \times 10^{23} \text{ erg s}^{-1}$, which is the typical luminosity of the detected sources. The results are shown in Figure 7. For both sets of binning we find a clear increase in the fraction of radio detections as a function of $v\sin i$, from a few percent at $v\sin i \lesssim 15 \text{ km s}^{-1}$ to about 30% at $v\sin i \gtrsim 30 \text{ km s}^{-1}$. This result suggests that while radio luminosity may not increase with faster rotation, the probability of producing radio emission does depend on fast rotation. This may be due to the influence of rotation on the magnetic field strength and/or its topology.

Studies of X-ray, Ca II H&K, and $\text{H}\alpha$ activity indicate that the Rossby number is the rotation parameter most highly closely correlated with magnetic activity (Noyes et al. 1984). We estimate the Rossby numbers for our sample using the method of Reiners & Basri (2010). The periods are estimated from $v\sin i$ combined with radii estimated from the mass-magnitude (Delfosse et al. 2000) and mass-radius (Baraffe et al. 1998) relations. A radius of $0.1 R_{\odot}$ is used for spectral types beyond M8. We estimate τ_c using the empirical relation of Kiraga & Stepien (2007) imposing a maximum of 70 d, consistent with Gilliland (1986). In Figure 8 we plot radio luminosity as a function of Ro . As in the case of radio luminosity versus $v\sin i$, we find no significant evolution from early-M to ultracool dwarfs. However, we note that the ultracool dwarfs with radio emission are clearly concentrated at $Ro \lesssim 5 \times 10^{-3}$, indicating that objects with low Rossby numbers are more likely to produce detectable radio activity.

In Figure 9 we plot the luminosity in radio, X-ray and $\text{H}\alpha$ scaled by the bolometric luminosity as a function of Ro . We supplement our data with results for F–K stars from the literature (Mekkaden 1985; Stewart et al. 1988; Slee & Stewart 1989; Delfosse et al. 1998; James et al. 2000; Pizzolato et al. 2003). The previously-discussed trends in X-ray and $\text{H}\alpha$ activity versus $v\sin i$ are more pronounced when plotted versus Rossby number. In particular, for spectral types earlier than M6 the X-ray activity exhibits a rapid increase by about 3 orders of magnitude as Ro decreases from ~ 2 to ~ 0.2 , followed by saturation at $Ro \lesssim 0.2$. The ultracool dwarfs exhibit a clear super-saturation trend of decreasing activity as a function of decreasing Rossby number in the range $Ro \approx 10^{-2}–10^{-3}$ (see also Berger et al. 2008). A similar trend is apparent in $\text{H}\alpha$ activity (see also Reiners & Basri 2010). On the other hand, in the radio band we find a uniform trend of increasing activity as a function of decreasing Rossby number over the range $Ro \approx 0.1–10^{-3}$ and for spectral types G to L, indicating that at least in some ultracool dwarfs, there is no evidence for a breakdown in the activity-Rossby number relation. A Spearman’s rank correlation test for the detected sources gives $\rho \approx -0.88$ with a null hypothesis (no correlation) probability of only $\approx 1.1 \times 10^{-15}$. A linear regression fit indicates an overall trend of $L_{\text{rad}}/L_{\text{bol}} \propto Ro^{-1.1}$.

Finally, Slee & Stewart (1989) noted the potential importance of radio surface flux (L_{rad}/R_*^2) as a quantity strongly correlated with rotation in G–K stars; here R_* is the stellar radius normalized to solar units. These authors found that $L_{\text{rad}}/R_*^2 \propto P^{-1.8 \pm 0.3} R_*^{1.8 \pm 0.4}$. In Figure 10 we plot radio surface flux as a function of Rossby number for the ultracool dwarfs in our sample and from the literature, as well as for the main sequence stars in the Slee & Stewart (1989) sample. The objects, ranging from spectral type G to L, again appear

to follow a single trend with respect to Ro . A Spearman's rank correlation test for the detected sources gives $\rho \approx -0.72$ with a null hypothesis (no correlation) probability of only $\approx 7.0 \times 10^{-8}$. A linear regression fit indicates an overall trend of $L_{\text{rad}}/R_*^2 \propto Ro^{-0.5}$.

5. IMPLICATIONS FOR MAGNETIC DYNAMO MODELS

The single trend of radio activity and surface flux as a function of Rossby number for G–L dwarfs, the overall increase in radio activity with rotation velocity, and the enhanced fraction of radio emitters at $v \sin i \gtrsim 25 \text{ km s}^{-1}$ indicate that rotation continues to play a role in the dynamo mechanism of ultracool dwarfs. These trends are at odds with observations in X-rays and $H\alpha$, which point to a breakdown in the relation between activity and rotation. This suggests that the reduced activity levels in X-rays and $H\alpha$ are due to external effects, such as the increased neutrality of the atmospheres, a reduction in the efficiency of bulk coronal heating, or centrifugal stripping, rather than to a substantial decrease in the dynamo efficiency. In this context, the radio observations provide strong support to Zeeman measurements that point to the continued presence of $\sim 1\text{--}3 \text{ kG}$ fields in some late-M dwarfs (Morin et al. 2010; Reiners & Basri 2010). However, ZDI measurements suggest a breakdown in the correlation between stellar parameters (e.g., rotation) and the field strength for $Ro \lesssim 0.1$ such that some rapid rotators have weak fields, while others have substantial fields (Morin et al. 2010). The evidence from radio observations extends to faster rotation velocities than the limit of $v \sin i \lesssim 20 \text{ km s}^{-1}$ for Zeeman measurements, and may be indicative of a similar trend, namely rapid rotators are more likely to produce radio emission, and to follow the same trend with respect to Rossby number of G–K stars, but there is a large fraction of rapid rotators with no detectable radio emission.

With the exception of the purely turbulent dynamo model of Durney et al. (1993), all other published models of fully-convective dynamos predict some level of relation between the magnetic energy density and rotation, at least up to a saturation level (Chabrier & Küker 2006; Dobler et al. 2006; Browning 2008). In particular, Chabrier & Küker (2006) find that for in an α^2 dynamo the resulting field strength depends on rotation up to a saturation value, and it may indeed dominate in the fastest rotators leading to the activity-rotation saturation observed in X-rays and $H\alpha$. Similarly, Dobler et al. (2006) find that on the large scales the magnetic energy increases with rotation (up to some saturation value), while small-scale fields are nearly independent of rotation. Browning (2008) also finds that faster rotators produce stronger fields, and that rapid rotation leads to suppression of differential rotation.

The dynamo models also predict that rotation will affect the field topology, but there is little agreement about the resulting field configurations. Predictions range from dominant axisymmetric fields (Browning 2008), with a primary quadrupolar component (Dobler et al. 2006), to large-scale, non-axisymmetric, high multipole order fields (Chabrier & Küker 2006). As in the case of field strength, field topology measurements with the ZDI technique suggest that in late-M dwarfs there is no clear correlation between stellar parameters (e.g., rotation) and the field topology. Since a substantial fraction of the radio emitters produce simple rotationally modulated emission indicative of a dipolar field topology (Berger et al. 2005; Hallinan et al. 2006, 2007; Berger et al. 2009; McLean et al. 2011), it is possible that magnetic topol-

ogy rather than field strength is the key to the change in the nature of magnetic activity among ultracool dwarfs, and that this is the main parameter that is correlated with rotation. A clear test of this possibility is to observe all radio emitters for at least a few rotation periods to test for periodicity. For the objects with $v \sin i \lesssim 20 \text{ km s}^{-1}$ this will require $\sim 40 \text{ hr}$ per source.

6. CONCLUSIONS

We presented new observations of a large sample of M and L dwarfs with measured rotation velocities aimed at addressing the radio activity-rotation relation in fully convective objects. This survey triples the number of ultracool dwarfs with measured rotation velocities and radio observations. As part of this survey we also discovered three new radio active ultracool dwarfs, of which one (2M1314+1320) exhibits periodic radio emission (McLean et al. 2011). Combining our observations with objects from the literature we find the following key results:

- In the M0–M6 dwarfs we find a saturation-type relation between rotation period and radio activity, similar to the one seen in $H\alpha$ and X-ray, and reaching saturation at a relatively low rotation velocity of about 5 km s^{-1} .
- Unlike the rapid decline in X-ray and $H\alpha$ activity in ultracool dwarfs, even for the most rapid rotators, the radio luminosity remains unchanged as a function of rotation velocity and spectral type, at least to spectral type of about L4. The ratio of radio to bolometric luminosity increases with later spectral type, well beyond the saturation value of M0–M6 dwarfs. However, as in the case of X-ray and $H\alpha$ activity we find an increased scatter in L_{rad} and $L_{\text{rad}}/L_{\text{bol}}$ for ultracool dwarfs.
- In the regime of fastest rotation ($v \sin i \gtrsim 20 \text{ km s}^{-1}$), there are fewer objects with low radio luminosity and a higher fraction of detected objects. This is contrary to the apparent X-ray and $H\alpha$ super-saturation in these fast rotators.
- The ratio of radio to bolometric luminosity and the radio surface flux increase as a function of decreasing Rossby number with a single trend for $Ro \sim 0.1\text{--}10^{-3}$ and spectral types G–L. This is in direct contrast to the saturated X-ray/ $H\alpha$ activity- Ro relation in G–L dwarfs, and the X-ray/ $H\alpha$ super-saturation in ultracool dwarfs.

Our most basic conclusion from these observations is that rotation continues to play a role in the magnetic activity of ultracool dwarfs, and hence in the underlying dynamo mechanism. It is not possible at the present to determine whether rotation mainly influences the field strength or its topology, since both may affect the detectability of radio emission. A clear test is long-term monitoring of the radio emitters to check for periodic modulation, which will allow us to reconstruct the field configuration (Berger et al. 2009; McLean et al. 2011). The ability of radio observations to trace the presence of magnetic fields in the most rapid rotators ($v \sin i \gtrsim 20 \text{ km s}^{-1}$) is particularly important in light of the inability of Zeeman measurements to probe this regime. We are clearly able to study the role of rotation down to $Ro \sim 10^{-3}$, while the Zeeman techniques are sensitive only to $Ro \gtrsim 10^{-2}$ (Morin et al. 2010; Reiners & Basri 2010).

While rotation clearly plays a role in radio activity, there are rapid rotators with no detectable radio emission, suggesting that more than one dynamo mechanism could be operating in ultracool dwarfs, or that the dynamo may lead to significantly different strengths/topologies. This is similar to the conclusion of Morin et al. (2010) from ZDI measurements of mid- and late-M dwarfs. In particular, it is possible that some rapid rotators are dominated by a dynamo that leads to a large-scale, low multipole order field that is more likely to result in detectable radio emission (particularly simple periodic radio emission). The long-term variability of at least some ultracool dwarfs (§3; Antonova et al. 2008; Berger et al. 2010) may be indicative of an episodic switch between the dynamo states.

Since most of the radio detections of ultracool dwarfs to date are close to the sensitivity limit of the VLA, future studies of individual objects and trends such as the activity-

rotation relation will greatly benefit from the order of magnitude increase in sensitivity afforded by the now-operational EVLA. Any constraints on the convective dynamo mechanism, atmospheric coupling of the magnetic field, or bulk coronal densities must take results from radio activity studies into account, particularly for the fastest rotators. In addition, theoretical dynamo models should explore the range of stellar parameters and rotation rates that are directly probed by radio observations, extending down to at least $Ro \sim 10^{-3}$.

E.B. acknowledges support for this work from the National Science Foundation through Grant AST-1008361. A.R. received research funding from the DFG as an Emmy Noether fellow (RE 1664/4-1). This work has made use of the SIMBAD database, operated at CDS, Strasbourg, France.

REFERENCES

- Antonova, A., Doyle, J. G., Hallinan, G., Bourke, S., & Golden, A. 2008, *A&A*, 487, 317
- Baraffe, I., Chabrier, G., Allard, F., & Hauschildt, P. H. 1998, *A&A*, 337, 403
- Basri, G., & Marcy, G. W. 1995, *AJ*, 109, 762
- Benz, A. O., & Guedel, M., 285, 621
- Berger, E. 2002, *ApJ*, 572, 503
- Berger, E. 2006, *ApJ*, 648, 629
- Berger, E., et al. 2001, *Nature*, 410, 338
- Berger, E., et al. 2010, *ApJ*, 709, 332
- Berger, E., et al. 2008, *ApJ*, 676, 1307
- Berger, E., et al. 2009, *ApJ*, 695, 310
- Berger, E., et al. 2005, *ApJ*, 627, 960
- Browning, M. K. 2008, *ApJ*, 676, 1262
- Browning, M. K., Basri, G., Marcy, G. W., West, A. A., & Zhang, J. 2010, *AJ*, 139, 504
- Burgasser, A. J., & Putman, M. E. 2005, *ApJ*, 626, 486
- Chabrier, G., & Küker, M. 2006, *A&A*, 446, 1027
- Cruz, K. L., Reid, I. N., Liebert, J., Kirkpatrick, J. D., & Lowrance, P. J. 2003, *AJ*, 126, 2421
- Delfosse, X., Forveille, T., Perrier, C., & Mayor, M. 1998, *A&A*, 331, 581
- Delfosse, X., Forveille, T., Ségransan, D., Beuzit, J.-L., Udry, S., Perrier, C., & Mayor, M. 2000, *A&A*, 364, 217
- Dobler, W., Stix, M., & Brandenburg, A. 2006, *ApJ*, 638, 336
- Donati, J.-F., Forveille, T., Collier Cameron, A., Barnes, J. R., Delfosse, X., Jardine, M. M., & Valenti, J. A. 2006, *Science*, 311, 633
- Durney, B. R., De Young, D. S., & Roxburgh, I. W. 1993, *Sol. Phys.*, 145, 207
- Faherty, J. K., Burgasser, A. J., Cruz, K. L., Shara, M. M., Walter, F. M., & Gelino, C. R. 2009, *AJ*, 137, 1
- Gilliland, R. L. 1986, *ApJ*, 300, 339
- Guedel, M., & Benz, A. O. 1993, *ApJ*, 405, L63
- Guedel, M., Schmitt, J. H. M. M., & Benz, A. O. 1995, *A&A*, 302, 775
- Hallinan, G., Antonova, A., Doyle, J. G., Bourke, S., Brisken, W. F., & Golden, A. 2006, *ApJ*, 653, 690
- Hallinan, G., et al. 2007, *ApJ*, 663, L25
- James, D. J., Jardine, M. M., Jeffries, R. D., Randich, S., Collier Cameron, A., & Ferreira, M. 2000, *MNRAS*, 318, 1217
- Jardine, M., & Unruh, Y. C. 1999, *A&A*, 346, 883
- Jenkins, J. S., Ramsey, L. W., Jones, H. R. A., Pavlenko, Y., Gallardo, J., Barnes, J. R., & Pinfield, D. J. 2009, *ApJ*, 704, 975
- Kiraga, M., & Stepien, K. 2007, *Acta Astron.*, 57, 149
- Krishnamurthi, A., Leto, G., & Linsky, J. L. 1999, *AJ*, 118, 1369
- McLean, M., Berger, E., Irwin, J., Forbrich, J., & Reiners, A. 2011, Submitted to *ApJ*; arXiv:1107.1516
- Mekkaden, M. V. 1985, *Ap&SS*, 117, 381
- Mohanty, S., & Basri, G. 2003, *ApJ*, 583, 451
- Mohanty, S., Basri, G., Shu, F., Allard, F., & Chabrier, G. 2002, *ApJ*, 571, 469
- Morin, J., Donati, J.-F., Petit, P., Delfosse, X., Forveille, T., & Jardine, M. M. 2010, *MNRAS*, 407, 2269
- Noyes, R. W., Hartmann, L. W., Baliunas, S. L., Duncan, D. K., & Vaughan, A. H. 1984, *ApJ*, 279, 763
- Parker, E. N. 1955, *ApJ*, 122, 293
- Phan-Bao, N., Osten, R. A., Lim, J., Martín, E. L., & Ho, P. T. P. 2007, *ApJ*, 658, 553
- Pizzolato, N., Maggio, A., Micela, G., Sciortino, S., & Ventura, P. 2003, *A&A*, 397, 147
- Reid, I. N., Kirkpatrick, J. D., Liebert, J., Gizis, J. E., Dahn, C. C., & Monet, D. G. 2002, *AJ*, 124, 519
- Reiners, A., & Basri, G. 2008, *ApJ*, 684, 1390
- Reiners, A., & Basri, G. 2010, *ApJ*, 710, 924
- Reiners, A., Basri, G., & Browning, M. 2009, *ApJ*, 692, 538
- Slee, O. B., & Stewart, R. T. 1989, *MNRAS*, 236, 129
- Stewart, R. T., Innis, J. L., Slee, O. B., Nelson, G. J., & Wright, A. E. 1988, *AJ*, 96, 371
- White, S. M., Jackson, P. D., & Kundu, M. R. 1989, *ApJS*, 71, 895

TABLE 1 — *Continued*

| 2MASS Number | Other Name | Sp.T. | J (mag) | K (mag) | d (pc) | $v \sin i$ (km s ⁻¹) | L_{bol} (L_{\odot}) | $L_{\text{H}\alpha}/L_{\text{bol}}$ | F_{ν} (μJy) | $\nu L_{\nu}/L_{\text{bol}}$ |
|-----------------|--------------|-------|--------------|--------------|-------------|-------------------------------------|-------------------------------------|-------------------------------------|---------------------------------|------------------------------|
| 0314034+160305 | | L0.0 | 12.53 | 11.24 | 14 | 19 | -3.59 | -4.69 | < 108 | < -6.66 |
| 1159385+005726 | | L0.0 | 14.08 | 12.81 | 30 | 71 | -3.57 | -5.06 | < 54 | < -6.35 |
| 1221277+025719 | | L0.0 | 13.17 | 11.95 | 19 | 25 | -3.59 | -4.88 | < 78 | < -6.54 |
| 1731297+272123 | | L0.0 | 12.09 | 10.91 | 12 | 15 | -3.56 | -4.80 | < 69 | < -7.03 |
| 1854459+842947 | | L0.0 | 13.66 | 12.47 | 23 | 7 | -3.62 | -4.73 | < 87 | < -6.29 |
| 1412244+163311 | | L0.5 | 13.89 | 12.52 | 25 | 19 | -3.61 | -5.50 | < 69 | < -6.33 |
| 1441371-094559 | | L0.5 | 14.02 | 12.66 | 28 | 23 | -3.59 | -5.48 | < 84 | < -6.20 |
| 2351504-253736B | | L0.5 | 12.47 | 11.27 | 18 | 41 | -3.36 | -5.22 | < 69 | < -6.87 |
| 0235599-233120 | | L1.0 | 13.67 | 12.19 | 21 | 13 | -3.63 | -6.44 | < 99 | < -6.30 |
| 1045240-014957 | | L1.0 | 13.16 | 11.78 | 17 | < 3 | -3.65 | -6.44 | < 57 | < -6.71 |
| 1048428+011158 | | L1.0 | 12.92 | 11.62 | 15 | 17 | -3.69 | -5.71 | < 21 | < -7.22 |
| 1439283+192914 | | L1.0 | 12.76 | 11.55 | 14 | 11 | -3.67 | -5.20 | < 78 | < -6.71 |
| 1555157-095605 | | L1.0 | 12.56 | 11.44 | 13 | 11 | -3.68 | -5.35 | < 84 | < -6.75 |
| 1145571+231729 | GL Leo | L1.5 | 15.39 | 13.95 | 44 | 14 | -3.70 | -5.27 | < 90 | < -5.65 |
| 1334062+194035 | | L1.5 | 15.48 | 14.00 | 46 | 30 | -3.68 | -6.53 | < 60 | < -5.74 |
| 1645221-131951 | | L1.5 | 12.45 | 11.15 | 12 | 9 | -3.69 | -5.66 | < 108 | < -6.71 |
| 1807159+501531 | 2MUCDä11756 | L1.5 | 12.93 | 11.62 | 15 | 76 | -3.71 | -5.26 | < 84 | < -6.62 |
| 0828341-130919 | | L2.0 | 12.80 | 11.30 | 14 | 33 | -3.64 | -6.63 | < 66 | < -6.83 |
| 0921141-210444 | DENIS-092114 | L2.0 | 12.78 | 11.69 | 12 | 15 | -3.83 | < -6.42 | < 75 | < -6.72 |
| 1029216+162652 | | L2.5 | 14.29 | 12.62 | 23 | 29 | -3.72 | -5.76 | < 33 | < -6.64 |
| 1047310-181557 | | L2.5 | 14.20 | 12.89 | 22 | 15 | -3.86 | -5.99 | < 63 | < -6.23 |
| 0913032+184150 | | L3.0 | 15.97 | 14.28 | 46 | 34 | -3.77 | -6.86 | < 102 | < -5.47 |
| 1203581+001550 | | L3.0 | 14.01 | 12.48 | 19 | 39 | -3.84 | -6.02 | < 63 | < -6.39 |
| 1506544+132106 | | L3.0 | 13.37 | 11.74 | 14 | 20 | -3.80 | -6.32 | < 78 | < -6.60 |
| 1615441+355900 | | L3.0 | 14.54 | 12.94 | 24 | 13 | -3.82 | < -5.98 | < 75 | < -6.13 |
| 1707234-055824 | 2MUCDä20701 | L3.0 | 13.96 | 12.25 | 17 | ... | -3.80 | ... | < 81 | < -6.42 |
| 0700366+315726A | | L3.5 | 13.23 | 11.62 | 12 | 41 | -3.88 | -6.04 | < 78 | < -6.39 |

NOTE. — Properties of the M and L dwarfs observed in this paper. The columns are (left to right): (i) 2MASS number; (ii) other name; (iii) spectral type; (iv) J -band magnitude; (v) K -band magnitude; (vi) distance from parallax or photometric estimate (from SIMBAD, Faherty et al. 2009, and Cruz et al. 2003); (vii) projected rotation velocity (from Mohanty & Basri 2003; Reid et al. 2002; Reiners & Basri 2008; Jenkins et al. 2009; Reiners & Basri 2010); (viii) bolometric luminosity; (ix) $\text{H}\alpha$ activity (from Delfosse et al. 1998; Mohanty & Basri 2003; Reiners & Basri 2008, 2010); (x) radio density flux; and (xi) ratio of radio to bolometric luminosity.

TABLE 2 — *Continued*

| 2MASS Number | Other Name | Sp.T. | J (mag) | K (mag) | d (pc) | $v \sin i$ (km s ⁻¹) | L_{bol} (L_{\odot}) | $L_{\text{H}\alpha}/L_{\text{bol}}$ | F_{ν} (μJy) | $\nu L_{\nu}/L_{\text{bol}}$ | Ref |
|-----------------|------------|-------|--------------|--------------|-------------|-------------------------------------|-------------------------------------|-------------------------------------|---------------------------------|------------------------------|-----|
| 2204105–564657B | | T6.0 | 13.23 | 13.53 | 4 | ... | –5.03 | ... | < 72 | < –6.58 | 2 |
| 1047539+212423 | | T6.5 | 15.82 | 16.41 | 11 | ... | –5.35 | ... | < 45 | < –6.26 | 2 |
| 1346464–003150 | | T6.5 | 16.00 | 15.77 | 15 | ... | –5.00 | ... | < 105 | < –5.23 | 5 |
| 0610351–215117 | GJ 229B | T7.0 | 14.20 | 14.30 | 6 | ... | –5.21 | ... | < 69 | < –6.01 | 4 |
| 1217111–031113 | | T7.5 | 15.86 | 15.89 | 11 | ... | –5.32 | ... | < 111 | < –5.13 | 2 |
| 0415195–093506 | | T8.0 | 15.70 | 15.43 | 6 | ... | –5.73 | ... | < 45 | < –5.68 | 2 |

NOTE. — Properties of the M, L, and T dwarfs from the literature. The columns are (left to right): (i) 2MASS number; (ii) other name; (iii) spectral type; (iv) J -band magnitude; (v) K -band magnitude; (vi) distance from parallax or photometric estimate (from SIMBAD, Faherty et al. 2009, and Cruz et al. 2003); (vii) projected rotation velocity (from Mohanty & Basri 2003; Reid et al. 2002; Reiners & Basri 2008; Jenkins et al. 2009; Reiners & Basri 2010); (viii) bolometric luminosity; (ix) $\text{H}\alpha$ activity (from Delfosse et al. 1998; Mohanty & Basri 2003; Reiners & Basri 2008, 2010); (x) radio density flux; (xi) ratio of radio to bolometric luminosity; and (xii) references for radio flux density measurements: [1] White et al. (1989); [2] Berger (2006); [3] Burgasser & Putman (2005); [4] Krishnamurthi et al. (1999); [5] Berger (2002); [6] Phan-Bao et al. (2007); [7] Berger et al. (2001); [8] Berger et al. (2009).

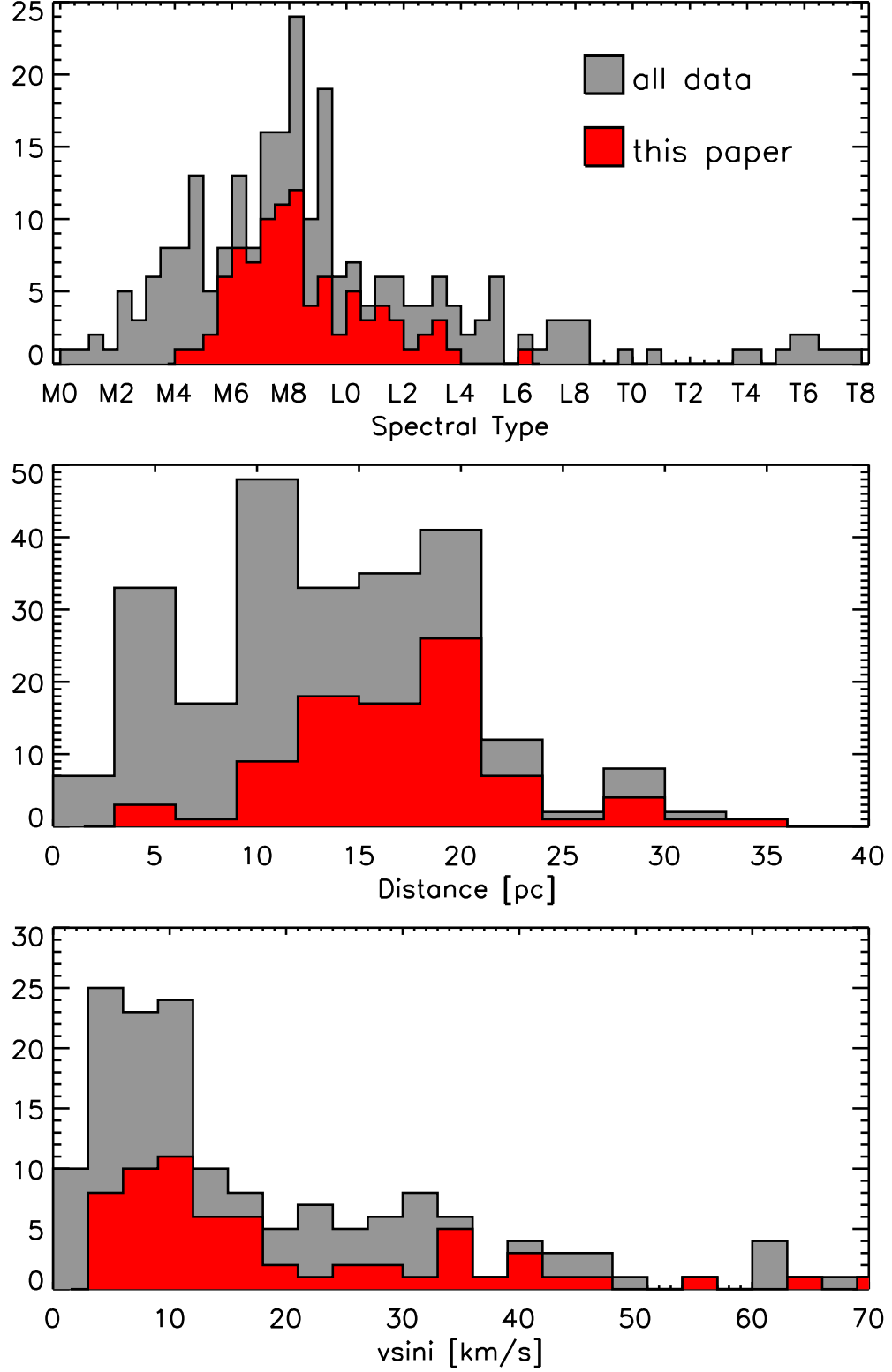


FIG. 1.— Properties of the survey sources, including spectral types (top), distances (middle), and projected rotation velocities (bottom). The new objects from this survey (Table 1) are shown in red while all data including observations from the literature (Table 2) are shown in gray.

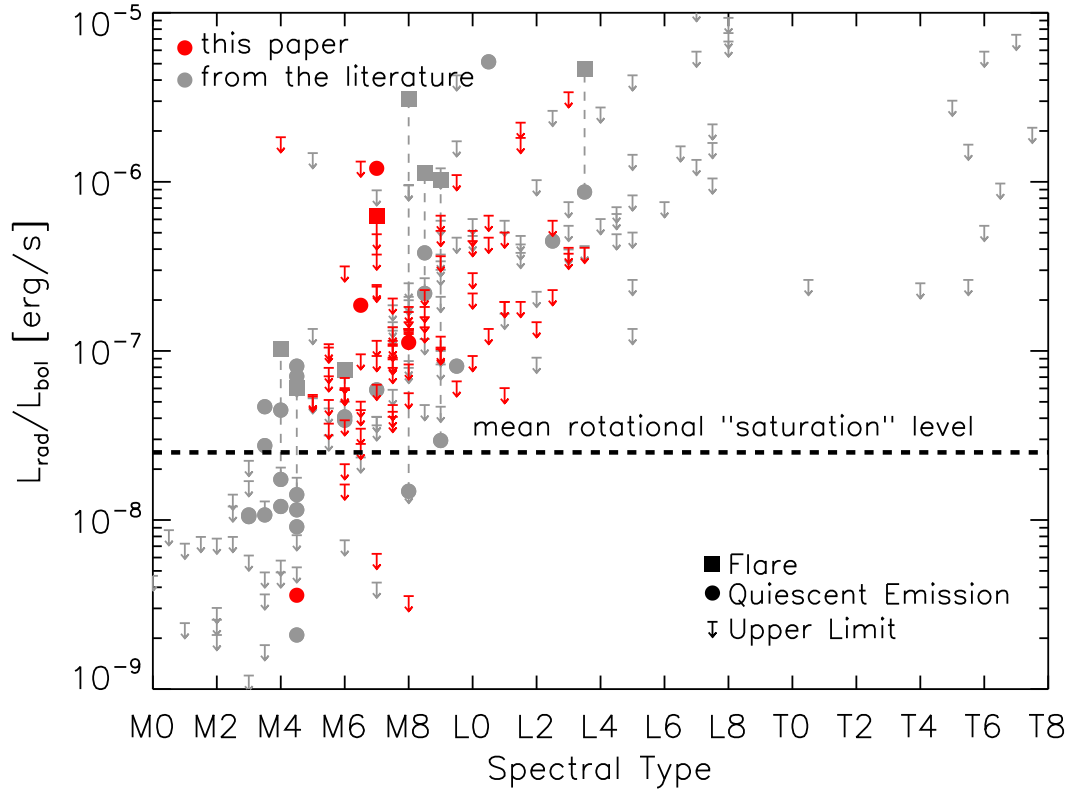


FIG. 2.— Ratio of radio to bolometric luminosity as a function of spectral type. Shown are flares (squares), quiescent emission (circles), and upper limits (arrows). Red symbols represent the objects from this survey (Table 1) while gray symbols represent objects from the literature (Table 2). The mean rotationally saturated level of emission for early- to mid-M dwarfs is shown as a dashed line (see Figure 5). The clear trend of increased $L_{\text{rad}}/L_{\text{bol}}$ as a function of later spectral type is seen in the ultracool dwarfs.

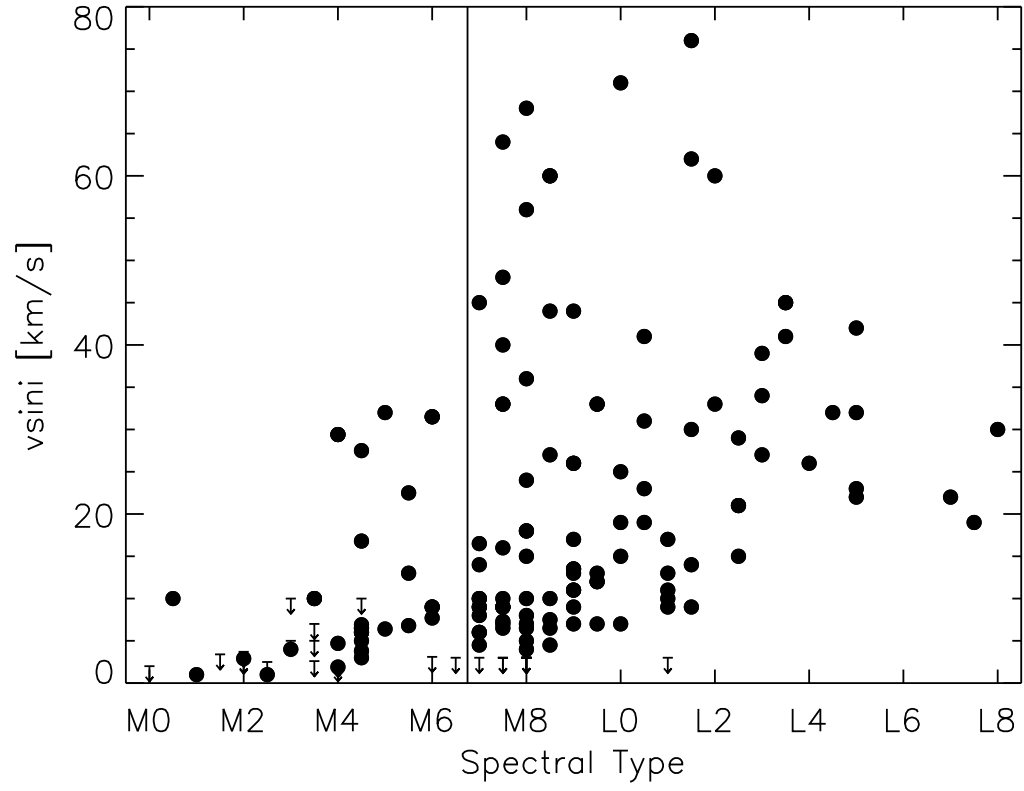


FIG. 3.— Projected rotation velocities ($v \sin i$) as a function of spectral type for the objects studied in this paper. The region above $v \sin i \approx 30 \text{ km s}^{-1}$ contains no early- or mid-M dwarfs, but is well populated by objects in the range M7–L5.

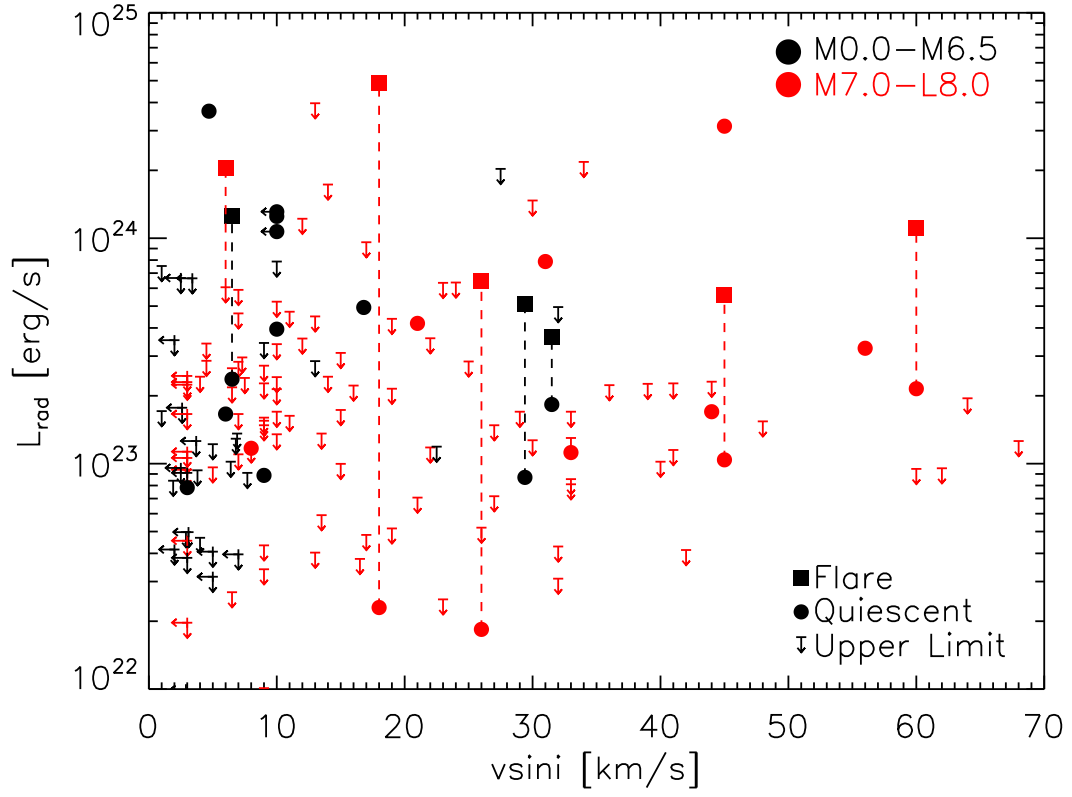


FIG. 4.— Radio luminosity as a function of projected rotation velocity. Shown are flares (squares), quiescent emission (circles), and radio upper limits (arrows). Left-arrows indicate upper limits in $v \sin i$. Red symbols represent objects later than M7, while black symbols represent objects with spectral types M0–M6.5. No obvious trend is detected, but there is a tantalizing paucity of objects with radio luminosity of $\lesssim 10^{23}$ erg s^{-1} at $v \sin i \gtrsim 30$ km s^{-1} .

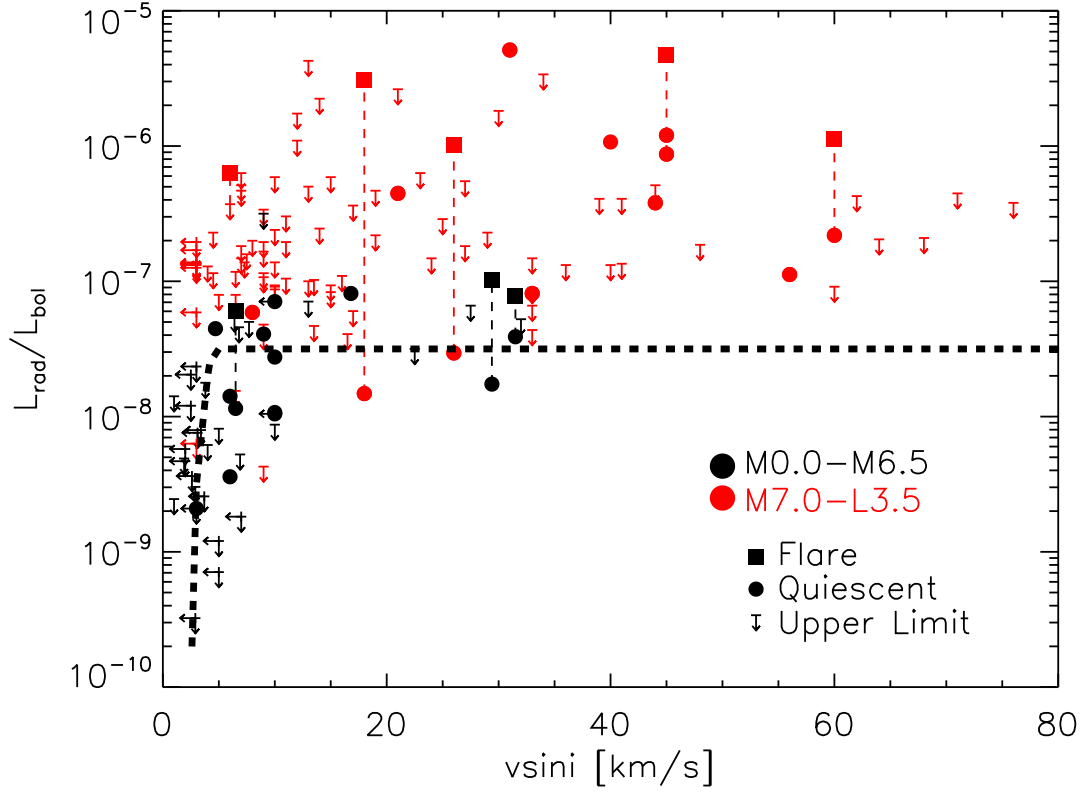


FIG. 5.— Ratio of radio to bolometric luminosity as a function of projected rotation velocity. Shown are flares (squares), quiescent emission (circles), and radio upper limits (arrows). Left-arrows indicate upper limits in $v\sin i$. Red symbols represent objects later than M7, while black symbols represent objects with spectral types M0–M6.5. The early- to mid-M dwarfs appear to reach a saturated level of $L_{\text{rad}}/L_{\text{bol}} \approx 10^{-7.5}$ at $v\sin i \gtrsim 5 \text{ km s}^{-1}$. The black dashed line indicates a rough fit to the radio activity-rotation relation for objects earlier than M7. There is a general increase in $L_{\text{rad}}/L_{\text{bol}}$ among the late-M and L dwarfs (as seen in Figure 2), as well as an increase in the scatter. There is also an indications of a trend towards higher luminosity ratios in the fastest rotators, $v\sin i \gtrsim 30 \text{ km s}^{-1}$.

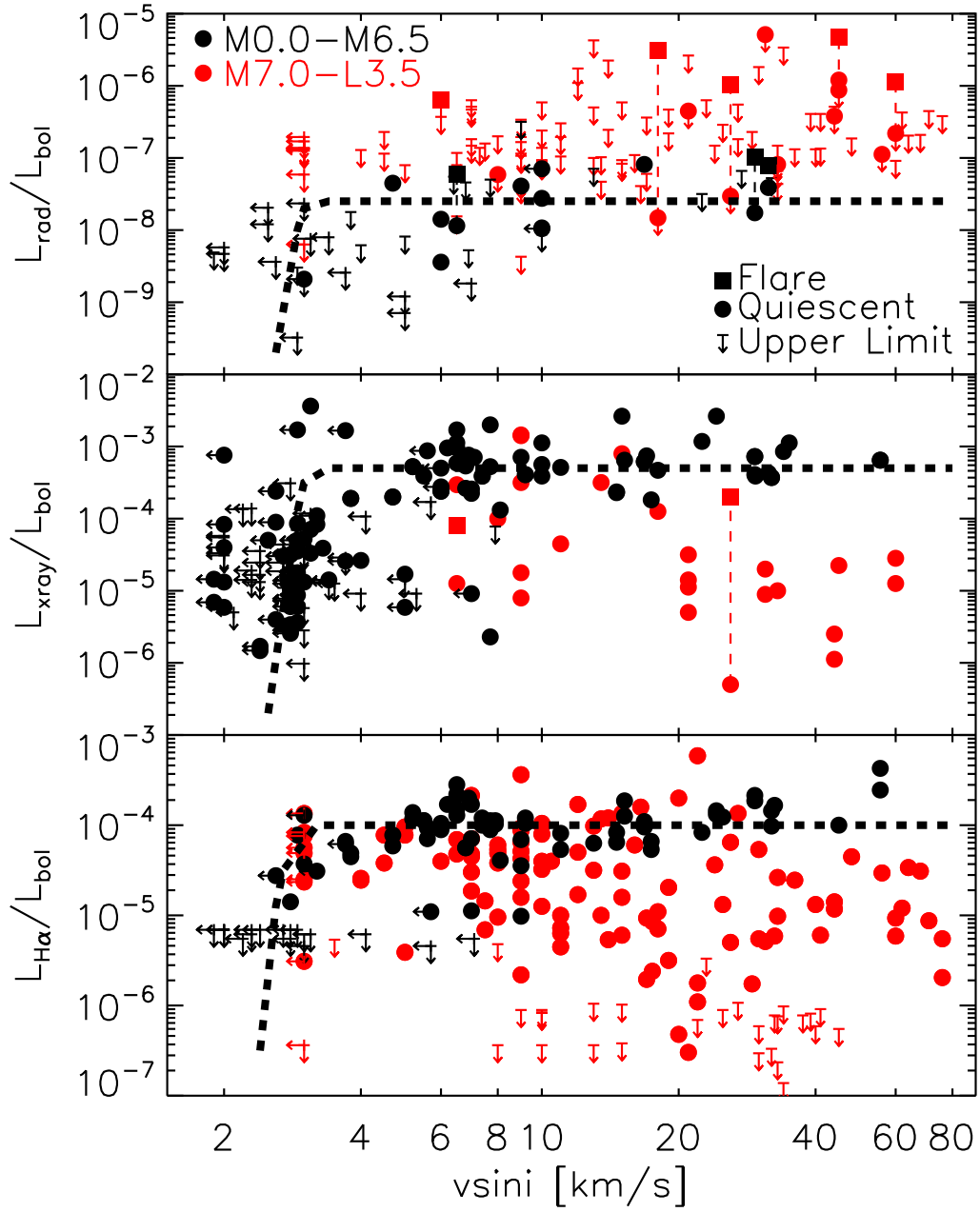


FIG. 6.— Radio, X-ray and $H\alpha$ activity as a function of projected rotation velocity. Shown are flares (squares), quiescent emission (circles), and upper limits (arrows). Left-arrows indicate upper limits in $v\sin i$. Red symbols represent objects later than M7, while black symbols represent objects with spectral types M0–M6.5. X-ray data are taken from Berger et al. (2008), James et al. (2000), Delfosse et al. (1998), and Pizzolato et al. (2003). $H\alpha$ data are taken from Delfosse et al. (1998), Mohanty & Basri (2003), Reiners & Basri (2008), and Reiners & Basri (2010). All three activity indicators appear to saturate at $\sim 5 \text{ km s}^{-1}$ for objects earlier than M6. The $H\alpha$ and X-ray activity-rotation relations break down at M7–M9 (Berger et al. 2008; Reiners & Basri 2010) with the activity dropping rapidly and the scatter increasing in later spectral types. There are hints of “super-saturation” above $\sim 30 \text{ km s}^{-1}$ where the luminosity drops in the most rapidly rotating objects. The radio activity follows a similar trend to the X-ray activity in the earlier objects. However, beyond M7, it begins to exhibit the opposite behavior.

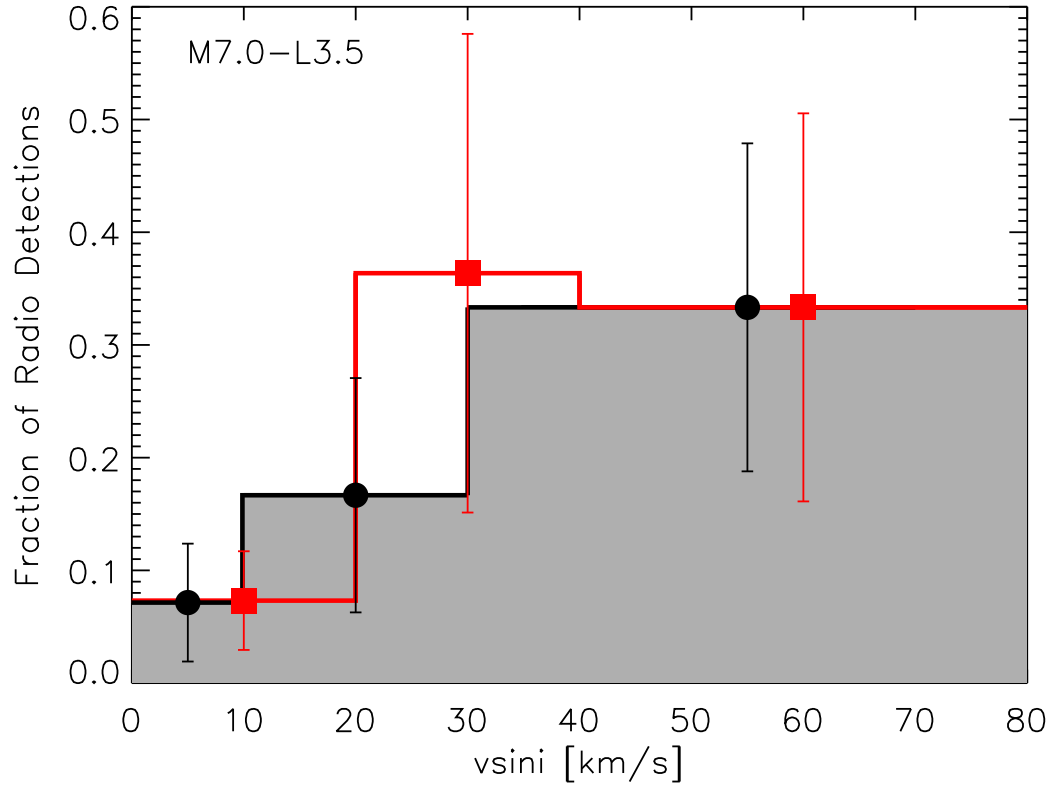


FIG. 7.— Fraction of objects with radio detections as a function of rotation velocity for ultracool dwarfs with spectral types M7–L4. Upper limits above $L_{\text{rad}} \approx 2.5 \times 10^{23} \text{ erg s}^{-1}$ have been excluded. Uncertainties are determined from the Poisson distribution. Two different sets of binning are shown in order to test the impact of the choice of boundaries. There is a clear increase in the fraction of detected objects among the fastest rotators. The transition seems to occur at $v \sin i \approx 20\text{--}30 \text{ km s}^{-1}$.

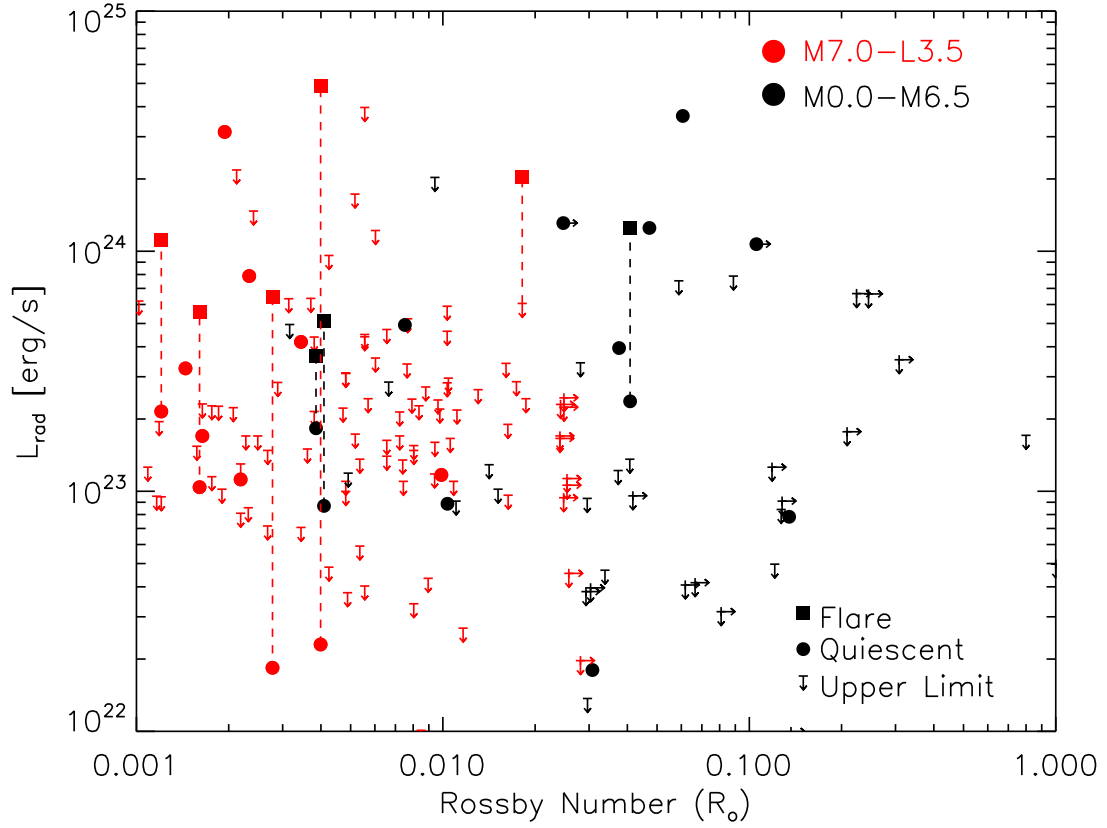


FIG. 8.— Radio luminosity as a function of Rossby number ($Ro = P/\tau_c$). Shown are flares (squares), quiescent emission (circles), and radio upper limits (arrows). Right-arrows indicate lower limits in Ro . Red symbols represent objects later than M7, while black symbols represent objects with spectral types M0–M6.5. As in Figure 4, no correlation between L_{rad} and Ro is obvious, but the bulk of ultracool dwarfs with radio detections are concentrated at low Rossby numbers, $Ro \lesssim 5 \times 10^{-3}$.

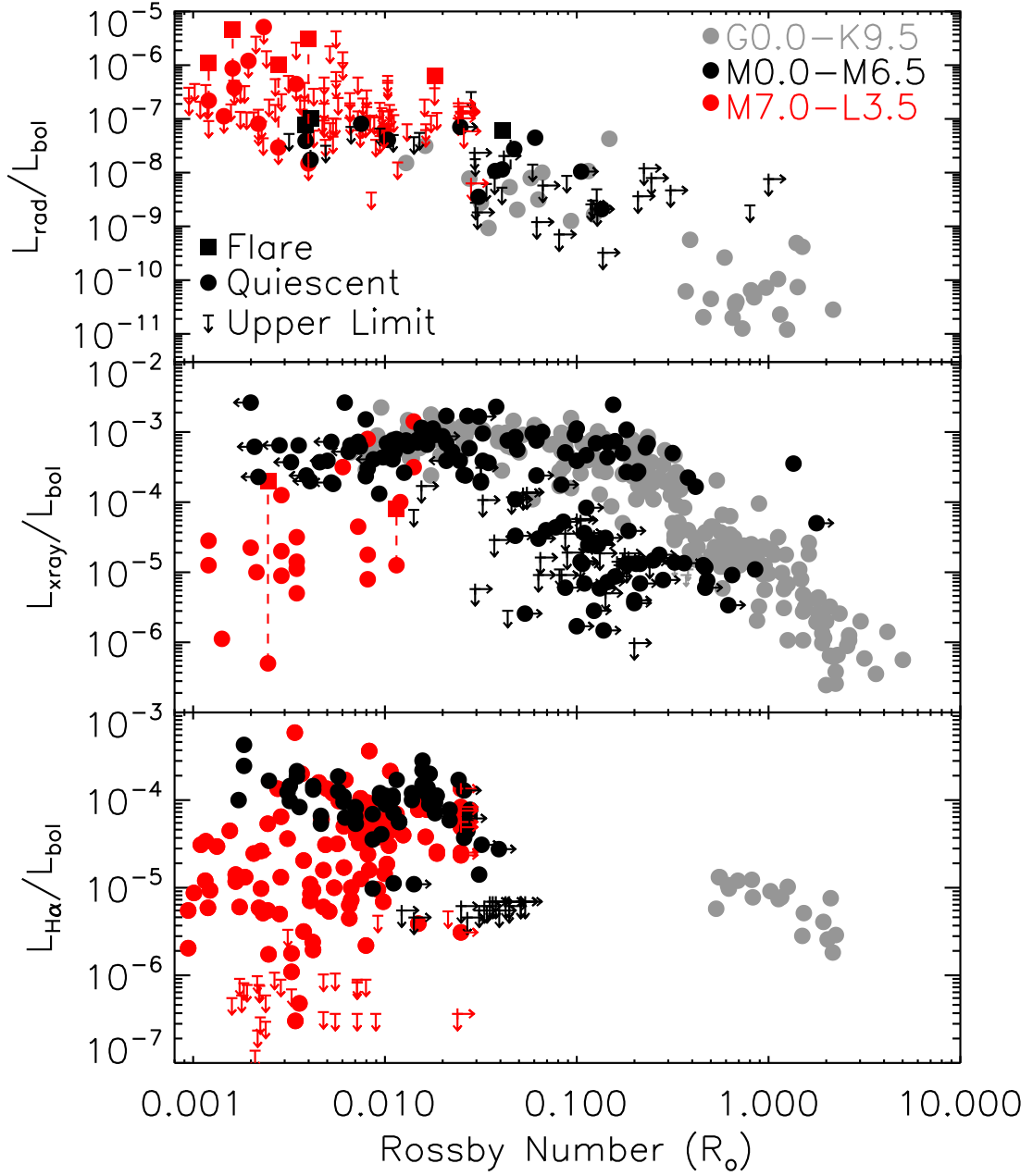


FIG. 9.— Radio, X-ray and H α activity as a function of Rossby number. Shown are flares (squares), quiescent emission (circles), and upper limits (arrows). Right-arrows indicate lower limits in R_o . Red symbols represent objects later than M7, black symbols represent objects with spectral types M0–M6.5, and gray symbols represent spectral types G–K. X-ray data are from James et al. (2000), Delfosse et al. (1998), Pizzolato et al. (2003), and Berger et al. (2008). H α data are from Meekaden (1985), Delfosse et al. (1998), Mohanty & Basri (2003), Reiners & Basri (2008), and Reiners & Basri (2010). Radio data for the G–K stars are from Stewart et al. (1988), Slee & Stewart (1989), and Guedel et al. (1995). As in Figure 6, the H α and X-ray activity-rotation relations break down at M7–M9 (Berger et al. 2008; Reiners & Basri 2010), with the activity dropping rapidly and the scatter increasing in later spectral types. There are hints of “super-saturation” in the most rapidly rotating ultracool dwarfs with $R_o \lesssim 0.01$. The radio activity appears to follow a single trend with Rossby number from M0–L4 and $R_o \approx 0.1 - 10^{-3}$.

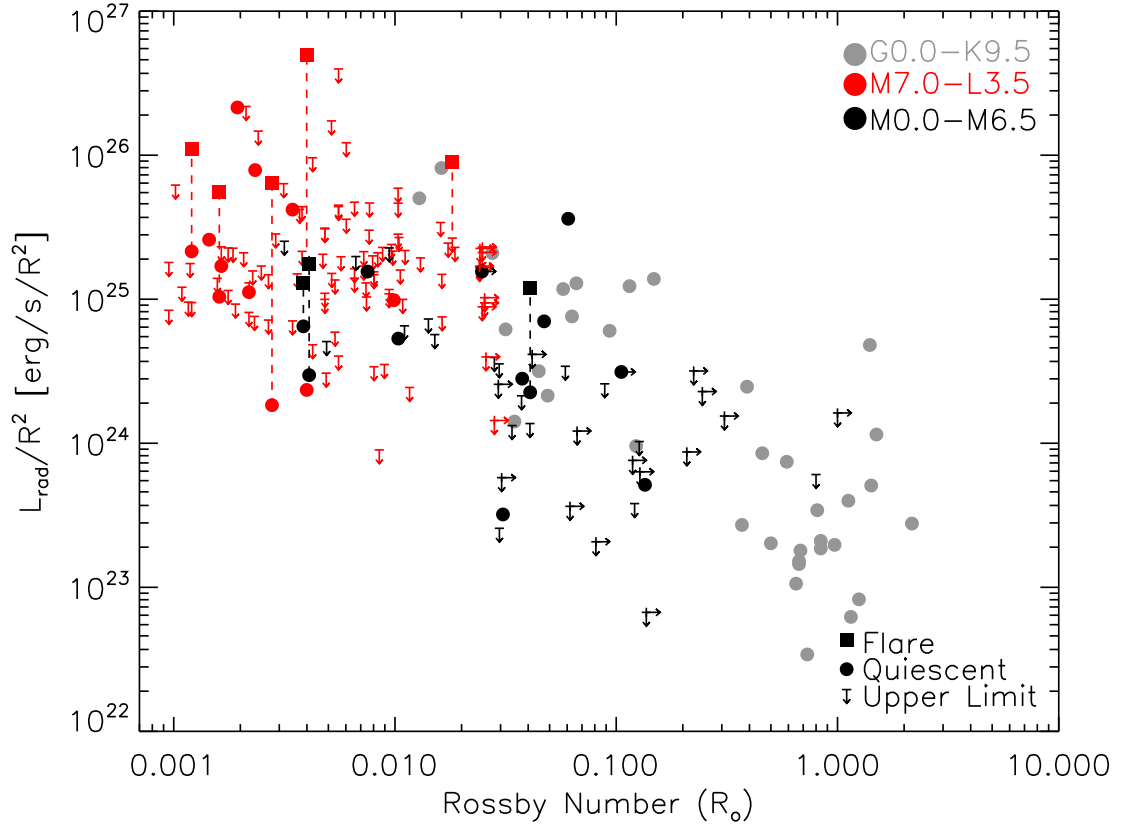


FIG. 10.— Radio surface flux as a function of Rossby number. Shown are flares (squares), quiescent emission (circles), and upper limits (arrows). Right-arrows indicate lower limits in R_o . Red symbols represent objects later than M7, black symbols represent objects with spectral types M0–M6.5, and gray symbols represent spectral types G–K (Stewart et al. 1988; Slee & Stewart 1989; Guedel et al. 1995). The stellar radii are in units of R_\odot . As in the case of $L_{\text{rad}}/L_{\text{bol}}$, the surface flux appears to follow a single trend from spectral types G2 to L4. The overall trend is roughly linear, $L_{\text{rad}}/R_*^2 \propto R_o^{-1}$.